

Observation of the supersolid stripe phase in spin-orbit coupled Bose-Einstein condensates

Junru Li^{*§}, Jeongwon Lee^{*}, Wujie Huang, Sean Burchesky, Boris Shteynas, Furkan Çağrı Top, Alan O. Jamison and Wolfgang Ketterle

Department of Physics, MIT-Harvard Center for Ultracold Atoms, and Research Laboratory of Electronics, MIT, Cambridge, Massachusetts 02139, USA

Supersolidity is an intriguing concept. It combines the property of superfluid flow with the long-range spatial periodicity of solids¹, two properties which are often mutually exclusive. The original discussion of quantum crystals² and supersolidity focuses on solid Helium-4 where it was predicted that vacancies could form dilute weakly interacting Bose-Einstein condensates^{1,3}. In this system, direct observation of supersolidity has been elusive[†]. The concept of supersolidity was then generalized to include other superfluid systems which break the translational symmetry of space. One of such systems is a Bose-Einstein condensate with spin-orbit coupling which has a supersolid stripe phase⁵⁻⁸. Despite several recent studies of this system^{9,10}, the stripe phase has not been observed. Here we report the direct observation of the predicted density modulation of the stripe phase using Bragg reflection. Our work establishes a system with unique symmetry breaking properties. Of future interest is further spatial symmetry breaking through the introduction of vortices^{11,12}, solitons¹³, impurities¹⁴ or disorder.

^{*} These authors contributed equally to this work.

[§] junruli@mit.edu

[†] Although the original observation of supersolidity³ turned out to be caused by unusual elastic properties, experiments still revealed quantum plasticity and mass supertransport, probably created by superfluid flow through the cores of interconnected dislocations^{1, 4}

Supersolids are defined as systems which spontaneously break two continuous, U(1), symmetries: the internal gauge symmetry by choosing the phase of the superfluid, and the translational symmetry of space by forming a density wave¹. With ultracold atoms, idealized Hamiltonians can be experimentally realized and studied. Starting from superfluid Bose-Einstein condensates (BECs), several forms of supersolids have been predicted by adding interactions in the form of dipolar interactions^{15, 16}, Rydberg interactions¹⁷, superradiant Rayleigh scattering¹⁸, nearest-neighbour interaction in lattices¹⁹ and spin-orbit interactions⁵⁻⁸. Several of these proposals lead to solidity along a single spatial direction. Breaking the translational symmetry for only one degree of freedom is analogous to liquid crystals. Supersolidity in BEC is an unusual form of matter as it combines gaseous, superfluid, and solid behaviours.

In a spin-orbit coupled Bose-Einstein condensate, the supersolid stripe phase emerges naturally in a description where spin-orbit coupling acts as a spin flip process with momentum transfer as shown in Fig. 1a. In solid-state materials, an electron moving at velocity \mathbf{v} through an electric field \mathbf{E} experiences a Zeeman energy term $-\mu_B \boldsymbol{\sigma} \cdot (\mathbf{v} \times \mathbf{E})$ due to the relativistic transformation of electromagnetic fields. The Zeeman term can be written as $\alpha_{ij} v_j \sigma_i / 4$ where the strength of the coupling α has the units of momentum. The $v_x \sigma_z$ term together with a transverse magnetic Zeeman term $\beta \sigma_x$ leads to the Hamiltonian $H = ((p_x + \alpha \sigma_z)^2 + p_y^2 + p_z^2) / 2m + \beta \sigma_x$. A unitary transformation shifts the momenta by $\alpha \sigma_z$ resulting in

$$H = \frac{P^2}{2m} + \begin{pmatrix} 0 & \beta e^{2i\alpha x} \\ \beta e^{-2i\alpha x} & 0 \end{pmatrix} \quad (1)$$

where the second term represents a spin flip process with a momentum transfer of 2α .

Therefore, spin-orbit coupling is equivalent to a spin flip process with momentum transfer which can be directly implemented for ultracold atoms using a two-photon Raman transition between the two spin states^{9,20}.

A Bose-Einstein condensate with equal populations in the two spin states shows no spatial interference due to the orthogonality of the two spin states. With spin-orbit coupling, each spin component has now two momentum components (0 and $\pm 2\alpha$) which form a stationary spatial interference pattern with a k vector of 2α (Fig.1a). Such spatial periodicity of the atomic density can be directly probed with Bragg scattering as shown in Fig. 1b. The position of the stripes is determined by the relative phase of the two condensates. This spontaneous phase breaks continuous translational symmetry. The two broken $U(1)$ symmetries are reflected in two Goldstone modes, one for density (or charge), the other one for spin transport²¹. Adding a longitudinal Zeeman term $\delta_0 \sigma_z$ to (1) leads to a rich phase diagram as a function of δ_0 and β ^{6,22}. For sufficiently large $|\delta_0|$, the ground state is in a plane wave phase. This phase has a roton gap^{10, 21} which decreases when $|\delta_0|$ is reduced, causing a roton instability and leading to a phase transition into the stripe phase.

Most experimental studies of spin-orbit coupling with ultracold atoms used two hyperfine ground states coupled by a two-photon Raman spin flip process^{9,10,23-26}. All previous studies with bosons used ^{87}Rb ^{9,10,27}. Alkali atoms, especially those with small fine structure splitting, suffer from heating due to spontaneous emission by the near resonant laser beams. Another possible limitation for observing the stripe phase is the required

miscibility of the two spin components. The difference in energy density between a BEC in the stripe phase and a phase-separated phase is $g \delta n^2 - (g - g_{\uparrow\downarrow}) n^2$ where g and $g_{\uparrow\downarrow}$ parameterize the interaction energy strengths between atoms in the same and in different spin states, respectively. The extra mean-field energy due to a modulation of the density n with amplitude δn leads to phase separation when the contrast of the stripes exceeds $\delta n / n = \sqrt{(g - g_{\uparrow\downarrow}) / g}$. For ^{87}Rb in the $|F=1, m_F=0\rangle$ and $|F=1, m_F=-1\rangle$ states, $(g - g_{\uparrow\downarrow}) / g = 10^{-3}$ is extremely small. In addition, the full width in δ_0 for stable stripes is $W = 2 n (g - g_{\uparrow\downarrow})$ which is $\sim 10\text{Hz}$ for ^{87}Rb and requires extreme control of ambient magnetic field fluctuations. For these reasons the stripe phase has not yet been observed in previous studies of ground state phases of the spin-orbit coupled system using rubidium atom^{9,10,27}.

All of these limitations were recently addressed by a new spin-orbit coupling scheme where orbital states (the lowest two eigenstates in an asymmetric double well potential) are used as the pseudospins²⁸. Since the eigenstates mainly populate the different wells, their interaction strength $g_{\uparrow\downarrow}$ is small and can be adjusted by adjusting their spatial overlap, improving the miscibility. Furthermore, since both pseudospin states have the same hyperfine state, there is no sensitivity to external magnetic fields. The scheme is realized with a coherently coupled array of double wells using an optical superlattice, a periodic structure with two lattice sites per unit cell with inter-site tunnelling J , as shown in Fig. 2a. The superlattice has two low lying bands, split by the energy difference Δ between the double wells, each hosting a BEC in the respective band minima. The BECs in the lower and upper band minimum are the pseudospin states in our system. Spin-orbit coupling is

created for the motion in the 2D plane orthogonal to the superlattice. In this work, we do not use the direction along the superlattice as a degree of freedom.

The experimental setup is described in ref. 28. Approximately 1×10^5 Bose-Einstein condensed ^{23}Na atoms were loaded into the optical superlattice along the z direction, equally split between the two pseudospin states with a density $n \sim 1.5 \times 10^{14} \text{ cm}^{-3}$. The superlattice consists of laser beams at $\lambda = 1064 \text{ nm}$ and 532 nm resulting in a lattice constant of $d = 532 \text{ nm}$. Spin-orbit coupling was induced by two $\lambda_{\text{IR}} = 1064 \text{ nm}$ Raman laser beams along the x and z axes, providing a momentum transfer $\hbar \mathbf{k}_{\text{Raman}} = \hbar (k_{\text{IR}}, 0, k_{\text{IR}})$ with two-photon Rabi frequency Ω . Here $k_{\text{IR}} = 2\pi/\lambda_{\text{IR}}$ is the recoil from a single Raman beam. The scheme realizes the spin-orbit Hamiltonian (1) with $\alpha = k_{\text{IR}}/2$, $\beta = (1/\sqrt{2})J\Omega/\Delta$, and an extra Zeeman term $\delta_0\sigma_z = (\delta - \Delta)/2 \sigma_z$ depending on the Raman beams detuning δ and superlattice offset Δ . J , Ω and Δ are determined from calibration experiments²⁸. The main addition to ref. 28 was a separate laser beam in the x - y plane for the detection of the supersolid stripes. The stripes form perpendicularly to the superlattice with a periodicity of $d_{\text{Stripe}} \approx \lambda_{\text{IR}} = 1064 \text{ nm}$. Their detection requires near resonant yellow light ($\lambda_{\text{Bragg}} = 589 \text{ nm}$) at an incident angle, $\theta = 16^\circ$, fulfilling the Bragg condition $\lambda_{\text{Bragg}} = 2 d_{\text{Stripe}} \sin(\theta)$. A major challenge was the alignment of this beam to an accuracy of better than $\sim 0.5^\circ$, the angular width of the Bragg signal, without any auxiliary density modulation at the same periodicity.* A second challenge was the smallness of the detected signal, on the order of 10 photons.

* Creating such a density modulation would have required a standing wave of laser light at 2128 nm .

Figure 1b shows the angular distribution of the Rayleigh scattered light induced by the 589 nm laser into the Bragg direction. The angular distribution is recorded by first focusing an imaging system onto the detection camera and then moving the camera out of focus. Without spin-orbit coupling, only Rayleigh scattering was observed (which has a broad dipolar angular pattern), filling the full aperture of the imaging system. The spin-orbit coupling leads to supersolid stripes and causes a specular reflection of the Bragg beam, observed as a sharp feature in the angular distribution of the Rayleigh scattered light (Fig 1b). The angular width (FWHM) of the observed peak of 9 ± 1 mrad is consistent with the diffraction limit of λ_{Bragg}/D , where D is the FWHM size of the cloud, demonstration long-range order of the stripes. This observation of the Bragg reflected beam is the main result of the paper, and constitutes a direct observation of the stripe phase.

Our detection of the stripe phase is almost background free, since all other density modulations have different directions, as depicted in Fig. 2. The superlattice is orthogonal to the stripes, along the z -axis. The Raman beams form a moving lattice and create a propagating density modulation at an angle of 45° to the superlattice in the $\hat{x} + \hat{z}$ direction. The pseudospin state in the upper band of the superlattice forms at the minimum of the band at a quasimomentum of $q = \pi / d$. The wave vector of the stripes is the sum of this quasimomentum and the momentum transfer that accompanies the spin flip of the spin-orbit coupling interaction²⁸, resulting in a stripe wave vector in the x direction. Since the difference in the wave vectors between the off-resonant density modulation and the stripes is not a reciprocal lattice vector, one cannot fulfil the Bragg condition simultaneously for both density modulations. In other spin-orbit coupling

schemes where the two pseudospins do not have different quasimomenta, the off-resonant density modulation and the stripes would be collinear. The background free Bragg detection of the stripes depends on the realization of a coherent array of spin-orbit coupled systems.

The amplitude of the stripes is predicted to be $\delta N/N_{\text{bec}} = 2\beta/E_r$ which is $\sim 8\%$ for $\beta = 300$ Hz where N_{bec} is the atom number in the condensates. Here $E_r = 7.6$ kHz is the ^{23}Na recoil energy for 1064 nm light. A sinusoidal density modulation of δN atoms gives rise to a Bragg signal proportional to $(\delta N)^2/4$, where $1/4$ is the structure factor for a sinusoidal modulation. Therefore, the ratio of the peak Bragg signal to the Rayleigh scattering background should be $(\delta N)^2/4N_{\text{tot}} = N_{\text{total}}(f\beta/E_r)^2$ where N_{total} is the total number of atoms and $f = N_{\text{bec}}/N_{\text{tot}}$ is the condensate fraction. For 10^5 atoms, the observed gain was 5 ± 1 with measured $f \approx 0.4$. The predicted value of 15 has an estimated uncertainty of a factor of two since calibration measurements and data taking were done on different days. At least some of the discrepancy is due to recoil heating by the Bragg beam which blurs the stripes, but does not reduce the Rayleigh scattering.

We observed a lifetime of about 20 ms for the Bragg signal after ramping up the spin-orbit coupling, accompanied by a clearly visible reduction in the number of atoms in the BEC. We believe that it is limited by the heating due to the Raman driving²⁸. At values of $\beta \approx 300$ Hz, the moving Raman lattice has a depth of $\sim 3 E_r$ which is comparable to the stationary lattice at $\sim 10 E_r$. When the spin-orbit coupling was increased further, the Bragg signal decreased, as shown in the inset of Fig. 3b, with noticeable atom loss. In addition,

the observed heating may still have a contribution from technical sources, since the observed lifetime is sensitive to alignment.

Fig. 3a shows the phase diagram for spin-orbit coupled BECs for the parameters implemented in this work. It features a wide area for the stripe phase, much larger than for ^{87}Rb , due to the high miscibility of the two orbital pseudospin states. The situation for our system and ^{87}Rb are complementary. In ^{87}Rb , the phase separated and the single minimum states have been studied⁹, whereas our scheme favours the stripe phase.

We explored the phase diagram in the vertical direction by varying the detuning δ of the two Raman beams. For $\delta_0 = 0$, the two dressed spin states are degenerate. For sufficiently large values of $|\delta_0|$, the ground state is the lower dressed spin state. The vertical width of the stripe phase in Fig. 3b depends on the miscibility of the two spin components^{6,22}. For our parameters, the equal population of the two pseudospin states is constant in a metastable way since the interactions between the two spin states are weak. This constraint of equal pseudospin populations leads to an effective detuning of $|\delta_0| = 0$. Therefore, the system remains in the stripe phase even for large detuning.

When the Raman beams detuning δ was varied, we observed peaked Bragg reflection at $\delta_0 \approx \pm 0.7E_r$ which were characterized earlier as spin flip resonances coupling $|\uparrow, q = 0\rangle$ to $|\downarrow, q = -k_{\text{IR}}\rangle$ and $|\downarrow, q = 0\rangle$ to $|\uparrow, q = k_{\text{IR}}\rangle$ (Fig 3b). The peaks in enhancement show that density modulations are resonantly created either in the $|\uparrow\rangle$ or $|\downarrow\rangle$ states. However, we observed a third sharper peak around $\delta_0 = 0$ which is not predicted by the mean field theory description. One possible explanation is that the stripes for non-zero δ_0 are moving

at a velocity δ_0/k_{IR} and therefore suffer from dissipation when they exceed the critical velocity for superfluidity. Using the speed of sound at the peak density as critical velocity suggests a four times wider peak. However, the critical velocities are lower in the spatial wings of the cloud. Another tentative explanation involves the alignment of the stripe patterns between different pancakes formed by the superlattice. Since the tunnel coupling along the superlattice direction is weak (about 1 kHz) it seems possible that the alignment of moving stripe patterns is more sensitive to perturbations than for stationary stripes.

The periodicity of the supersolid density modulation can depend on external, single-atom and two atom parameters. In the present case, the periodicity is given by the wavelength and geometry of the Raman beams. It is then further modified by the spin gap parameter β and the interatomic interactions^{5, 6}

$$d_{\text{stripe}} = \frac{\lambda_{\text{IR}}}{\sqrt{1 - \frac{\beta^2}{F^2}}} \quad (2)$$

where $F = (2E_r + n(g + g_{\uparrow\downarrow}))/4$. For $\beta \sim 300\text{Hz}$, the difference between d_{stripe} and λ_{IR} is only 0.4% and was not detectable in our work. In the case of dipolar supersolids, the periodicity of the density modulation is determined by the strength of the two-body dipolar interactions^{15, 16}. For supersolids created by superradiant Rayleigh scattering, the periodicity is half the wavelength of the scattered light, but modified by the atomic density through the index of refraction¹⁸.

In the case of a lattice supersolid, the spatial period is an integer multiple of the external lattice thereby breaking a discrete translational symmetry²⁹. In our system we also

observe this kind of supersolidity. Here, the density modulation occurs in the superlattice without spin-orbit coupling. As discussed in our previous work²⁸, the two BECs in the two pseudospin states have different quasimomenta q in the superlattice, one being at $q = 0$ in the lowest band, the other at $q = 2\pi / \lambda_{\text{IR}}$ at the Brillouin zone boundary in the upper band. The difference in quasimomenta implies an xy antiferromagnetic pseudospin texture, doubling the period of the superlattice²⁸. Due to tunnelling between the two wells, this spin texture leads to a density modulation with the same spatial periodicity (Fig 4) with maximum amplitude (J/Δ) . This density modulation breaks the translational symmetry of the lattice, and therefore fulfils the definition of a lattice supersolid^{1, 29}, where a discrete translational symmetry is spontaneously broken. With the same periodicity of 1064 nm as the supersolid stripe phase, this density modulation can be detected with the same geometry of the Bragg beam and camera, but rotated to the y-z plane. Figure 4b shows the observed enhanced light scattering due to Bragg reflection. The Bragg signal was absent right after preparing an equal mixture of the two pseudospin states, both in $q = 0$, and appeared spontaneously after the upper pseudospin state relaxed to the band minimum at $q = 2\pi / \lambda_{\text{IR}}$. The antiferromagnetic spin texture is rotating at frequency Δ , the energy offset between the two pseudospin states, which causes a temporal oscillation of the density modulation with spontaneous initial phase. With Bragg pulse duration shorter than $1/2\Delta$, the Bragg signal varied between 0 and 100 %, depending on the phase of the oscillation of the density modulation when probed. The increased fluctuation in Fig. 4b shows the random nature of the initial phase, which is consistent with spontaneous symmetry breaking.

In conclusion, we have observed the long-predicted supersolid phase of spin-orbit coupled Bose-Einstein condensates. This realizes a well-understood system which simultaneously has off-diagonal and diagonal long-range order. In the future, it will be interesting to characterize this system by its collective excitations²¹ and to find ways to extend it to two-dimensional spin-orbit coupling which leads to a different and rich phase diagram³⁰⁻³². Another direction of the future research is the study of vortices and the effects of impurities and disorder in different phases of spin-orbit coupled condensates¹¹⁻¹⁴.

Note: When we presented this work at a workshop in Chicago on 9/26, we learnt about related unpublished work on supersolidity which subsequently appeared as a preprint. See Léonard, J., Morales, A., Zupancic, P., Esslinger T. & Donner, T. Supersolid formation in a quantum gas breaking continuous translational symmetry. arXiv: 1609.09053v1 (2016).

References

1. Boninsegni, M. & Prokof'ev, N. V. Colloquium: Supersolids: What and where are they? *Rev. Mod. Phys.* **84**, 759 (2012).
2. Chester, G. V. Speculations on Bose-Einstein Condensation and Quantum Crystals. *Phys. Rev. A* **2**, 256 (1970).
3. Kim, E. & Chan, M.H.W. Probable observation of a supersolid helium phase. *Nature* **427**, 225-227 (2004).
4. Kuklov, A. B., Pollet, L., Prokof'ev, N.V. & Svistunov, B.V. Quantum plasticity and supersolid response in helium-4. *Phys. Rev. B* **90**, 184508 (2014)

5. Li, Y., Pitaevskii, L. P. & Stringari, S. Quantum Tricriticality and Phase Transitions in Spin-Orbit-Coupled Bose-Einstein Condensates. *Phys. Rev. Lett.* **108**, 225301 (2012).
6. Ho, T.-L., & Zhang, S. Bose-Einstein Condensates with Spin-Orbit Interaction. *Phys. Rev. Lett.* **107**, 150403 (2011).
7. Zhai, H. Spin-Orbit Coupled Quantum Gases. *Int. J. Mod. Phys. B*, **26**, 1230001 (2012).
8. Wang, C., Gao, C., Jian, C.-M. & Zhai, H. Spin-Orbit Coupled Spinor Bose-Einstein Condensates. *Phys. Rev. Lett.* **105**, 160403 (2010).
9. Lin, Y.-J., Jiménez-García, K. & Spielman, I. B. Spin-Orbit-coupled Bose-Einstein condensates. *Nature* **471**, 83-86 (2010).
10. Ji, S.-C. *et al.* Softening of Roton and Phonon Modes in a Bose-Einstein Condensate with Spin-Orbit Coupling. *Phys. Rev. Lett.* **114**, 105301 (2015)
11. Kasamatsu, K. dynamics of quantized vortices in Bose-Einstein condensates with laser-induced spin-orbit coupling. *Phys. Rev. A* **92**, 063608 (2015).
12. Su, S.-W. *et al.* Position-dependent spin-orbit coupling for ultracold atoms. *New J. Phys.* **17** 033045 (2015).
13. Fialko, O., Brand, J. & Zülicke, U. Soliton magnetization dynamics in spin-orbit-coupled Bose-Einstein condensates. *Phys. Rev. A* **85**, 051605(R) (2012).

14. Zheng, W., Yu, Z.-Q., Cui, X. & Zhai, H. Properties of Bose gases with the Raman-induced spin-orbit coupling. *J. Phys. B: At. Mol. Opt. Phys.* **46** 134007 (2013).
15. Giovanazzi, S., O'Dell, D. & Kurizki, G. Density Modulations of Bose-Einstein Condensates via Laser-Induced Interactions. *Phys. Rev. Lett.* **88**, 130402 (2002).
16. Góral, K., Santos, L. & Lewenstein, M. Quantum Phase of Dipolar Bosons in Optical Lattice. *Phys. Rev. Lett.* **88**, 170406 (2002).
17. Henkel, N., Nath, R. & Pohl, T. Three-Dimensional Roton Excitations and Supersolid Formation in Rydberg-Excited Bose-Einstein Condensates. *Phys. Rev. Lett.* **104**, 195302 (2010).
18. Ostemann, S., Piazza, F. & Ritsch, H. Spontaneous Crystallization of Light and Ultracold Atoms. *Phys. Rev. X* **6**, 021026 (2016).
19. Wessel, S. & Troyer, M. Supersolid Hard-Core Bosons on the Triangular Lattice. *Phys. Rev. Lett.* **95**, 127205 (2005).
20. Stanescu, T.D., Anderson, B. & Galitski, V. Spin-orbit coupled Bose-Einstein condensates. *Phys. Rev. A* **78**, 023616 (2008).
21. Li Y., Martone, G. I., Pitaevskii, L. P. & Stringari, S. Superstripes and the Excitation Spectrum of a Spin-Orbit-Coupled Bose-Einstein Condensate. *Phys. Rev. Lett.* **110**, 235302 (2013).
22. Martone, G. I. Visibility and stability of superstripes in a spin-orbit-coupled Bose-Einstein condensate. *Eur. Phys. J. Special Topics* **224**, 553-563 (2015).

23. Burdick, N. Q., Tang, Y. & Lev, B. Long-Lived Spin-Orbit-Coupled Degenerate Dipolar Fermi Gas. *Phys. Rev. X* **6**, 031022 (2016).
24. Cheuk, L. W. *et al.* Spin-Injection Spectroscopy of a Spin-Orbit Coupled Fermi Gas. *Phys. Rev. Lett.* **109**, 095302 (2012).
25. Wang, P. *et al.* Spin-Orbit Coupled Degenerate Fermi Gases. *Phys. Rev. Lett.* **109**, 095301 (2012).
26. Song, B. *et al.* Spin-orbit coupled two-electron Fermi gases of ytterbium atoms. *arXiv*: 1608.00478v2 (2016).
27. Ji, S.-C. *et al.* Experimental determination of the finite-temperature phase diagram of a spin-orbit coupled Bose gas. *Nature Phys.* **10**, 314-320 (2014).
28. Li, J. *et al.* Spin-Orbit Coupling and Spin Textures in Optical Superlattices. *arXiv*:1606.03514v1 (2016) accepted to *Phys. Rev. Lett.*
29. Chen, Y., Ye, J. & Tian, G. Classification of a Supersolid: Trial Wavefunctions, Symmetry breaking and Excitation Spectra. *J. Low. Temp. Phys.* (2012) 169:149-168
30. Sinha, S., Nath, R. & Santos, L. Trapped Two-Dimensional Condensates with Synthetic Spin-Orbit Coupling. *Phys. Rev. Lett.* **107**, 270401 (2011).
31. Gopalakrishnan, S., Lamacraft, A. & Golbart, P.M. Universal phase structure of dilute Bose gases with Rashba spin-orbit coupling. *Phys. Rev. A* **84**, 061604(R) (2011).

32. Sun, Q., Wen, L., Liu, W.-M., Juzeliūnas, G. & Ji, A.-C. Tunneling-assisted spin-orbit coupling in bilayer Bose-Einstein condensates. *Phys. Rev. A* **91**, 033619 (2015).

Acknowledgments We acknowledge helpful discussions with S. Stringari. We thank W. C. Burton for carefully reading the manuscript. We thank the support from the NSF through the Center for Ultracold Atoms and by award 1506369, from ARO-MURI Non-equilibrium Many-body Dynamics (grant W911NF-14-1-0003) and from AFOSR-MURI Quantum Phases of Matter (grant FA9550-14-1-0035)

Author contributions All authors contributed to the writing of the manuscript. J. Li, W. H., J. Lee, B. S., S. B., F. C. T., and A. O. J. contributed to the building of the experiment. J. Li led the data taking efforts. J. Lee led the data analysis and simulations. W. H., J. Li, and W. K. conceived the experiment.

Competing financial interests The authors declare no competing financial interests.

Author Information Correspondence and requests for materials should be addressed to J. Li. (junruli@mit.edu).

Methods

Sample preparation We prepared $N \approx 4 \times 10^5$ ^{23}Na atoms in a crossed optical dipole trap. An equal mixture of spin up and spin down states is created using the method described in our earlier work²⁸. The superlattice is adiabatically ramped up with an offset $\Delta = 0$. The final offset is then rapidly set by a fast frequency change of the infrared lattice. The offset is determined by the intensity of the $\lambda = 1064$ nm lattice laser light and the relative phase ϕ_{SL} between the two lattices. The offset Δ is calibrated with the method described in ref. 28. We estimate the stability of the offset parameter Δ to be 1 kHz limited by drifts in the air pressure which affect the relative phase ϕ_{SL} between the two lattices. Subsequently, the Raman lasers inducing the spin-orbit coupling are adiabatically ramped up within ~ 10 ms followed by a variable hold time, after which the Bragg probe beam is pulsed.

Bragg beam parameters and detection The Bragg beam was chosen to be ~ 1030 MHz blue detuned from the sodium $|3S_{1/2}, F = 1\rangle$ to $|3P_{3/2}, F = 2\rangle$ transition with a linear polarization along the superlattice direction. The detuning was chosen such that the Bragg beam can propagate through the entire condensate without significant absorption or wave front distortions.

The Bragg reflected beam and the fluorescence were recorded with an EMCCD camera. The signal was normalized for fluctuating atom numbers using the Rayleigh scattering intensity monitored by a photomultiplier tube using a separate viewport.

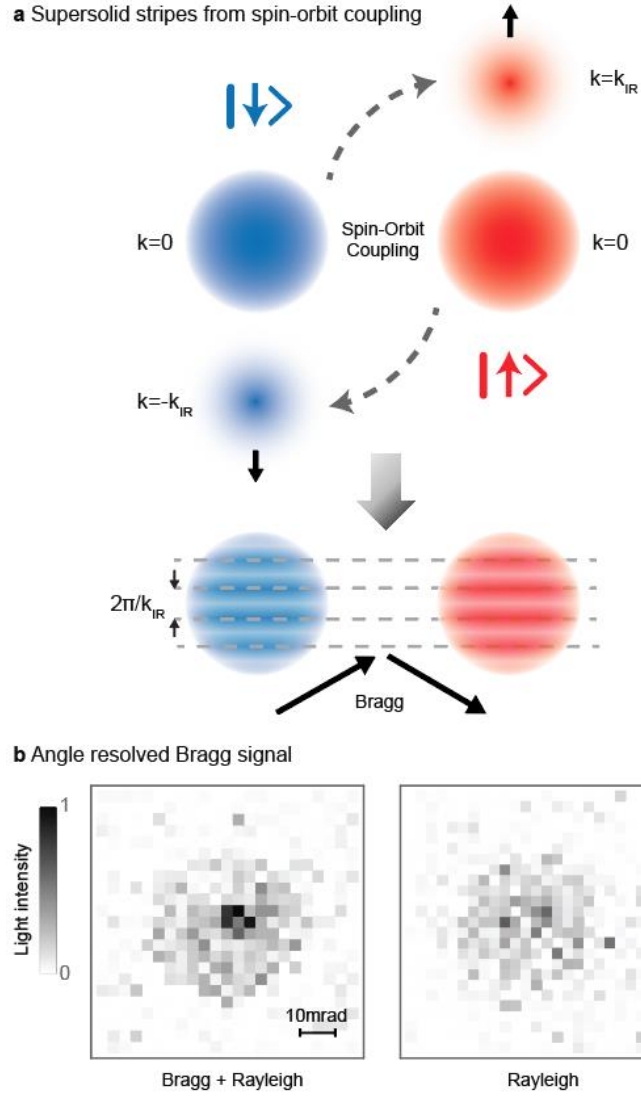


Figure 1 | Origin of supersolid stripes and detection via Bragg scattering. **a**, Spin-orbit coupling adds momentum components, $\pm k_{\text{IR}}$, of the opposite spin state to the spin up and spin down Bose Einstein condensates (top panel: spin states in momentum space). Matter wave interference leads to a spatial density modulation of period $2\pi/k_{\text{IR}}$ (bottom panel: spin states in real space). The spatial periodicity can be directly probed by Bragg scattering. **b**, Detection of the supersolid stripe phase by angle resolved light scattering. A sharp specular feature in the left panel is the Bragg signal due to the periodic density modulation. The diffuse signal is Rayleigh scattering filling the round aperture of the imaging system. Without spin-orbit coupling, only Rayleigh scattering is observed (right panel). The figure is the average over seven shots.

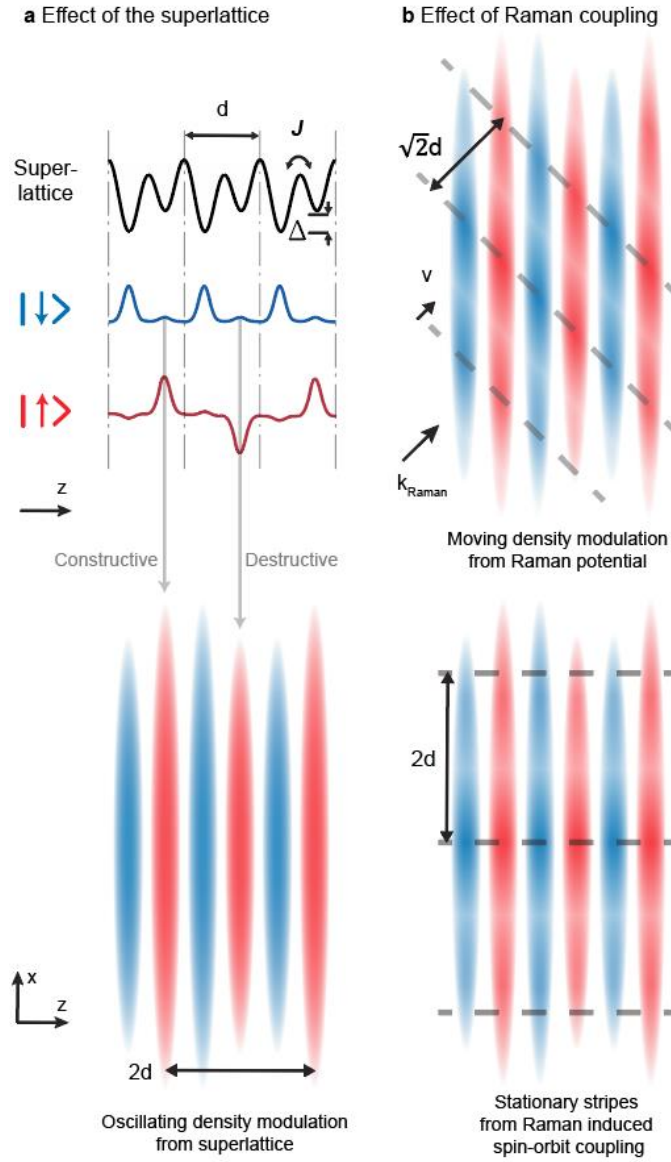


Figure 2 | Three types of density modulations present in our system. **a**, The two lowest bands of the superlattice are mapped into orbital pseudospins. The interference between the pseudospin down and up states alternates between constructive and destructive for adjacent unit cells in the lattice. This generates an oscillating density modulation with spatial periodicity of $2d$ along the superlattice direction (z axis). **b**, Coupling the pseudospins with Raman laser beams causes two different types of density modulations; one is a moving density modulation caused by the moving lattice potential, and the other is the stationary stripes from Raman induced spin-orbit coupling between the pseudospins.

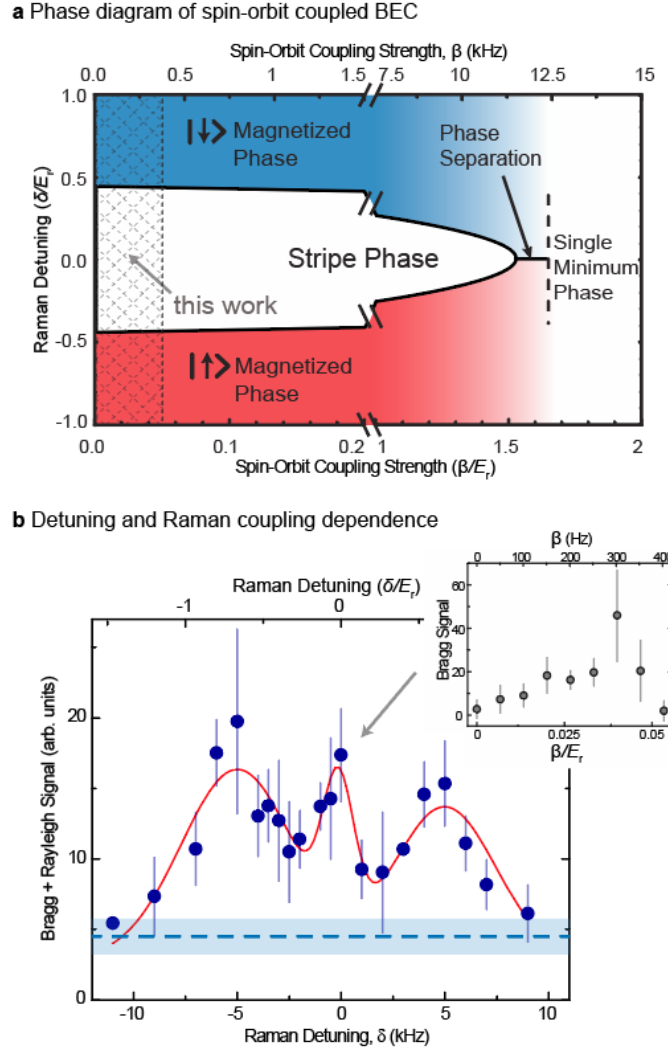


Figure 3 | Phase diagram for spin-orbit coupled Bose-Einstein condensates, and effect of Raman detuning and intensity on the supersolid stripes. **a**, Mean-field phase diagram of spin-orbit coupled Bose-Einstein condensates as a function of Raman detuning and spin-orbit coupling strength. The parameter space explored in this work is shown in grey crosshatch lines. However, due to metastability, our effective detuning is always zero (see text). **b**, Dark blue filled circles show the total light scattering signal (Bragg and Rayleigh) as a function of the frequency detuning. The light was detected within a solid angle of 10 mrad. The light blue dashed line and shaded area show the mean and standard deviation of the Rayleigh scattered light for the same conditions. The red solid line is a triple Gaussian fit to the total light scattering where the widths and center positions of the two outer peaks are constrained to be identical to the spin flip resonances studied in our previous work²⁸. **Inset**, Bragg scattering signal versus Raman coupling strength at zero Raman detuning.

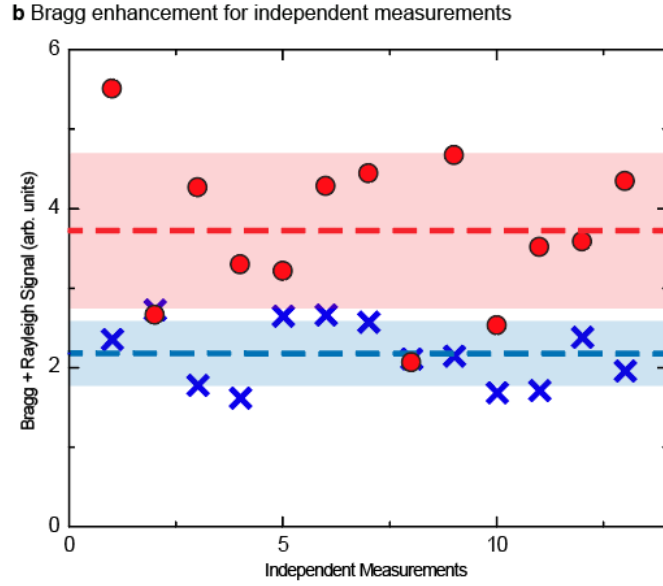
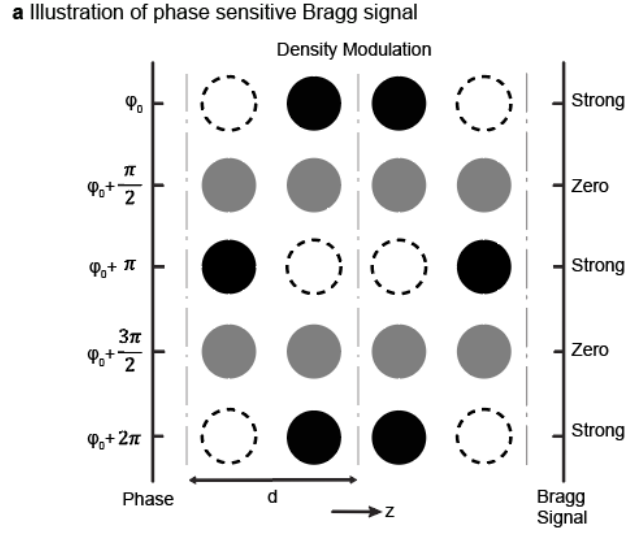


Figure 4 | Bragg detection of a lattice supersolid caused by an antiferromagnetic spin texture. **a**, Density modulation along the superlattice direction is shown for different relative phases between the orbital pseudospins, $\varphi = \varphi_0 + \Delta t$ (only the case of φ_0 and $\varphi_0 + 2\pi$ are shown in Fig. 2a). The Bragg signal depends on the relative phase when the Bragg pulse width is shorter than $1/(2\Delta)$. **b**, Blue x's show the Rayleigh scattered background before the antiferromagnetic spin texture develops. Red filled circles show Bragg enhanced scattering, which is set up to detect a density modulation of periodicity $2d$ along the superlattice direction. The Bragg enhancement fluctuated between zero and a factor of two, which indicates variations of the spontaneous phase φ_0 , between independent measurements.